

Electrical conductivity and partial melting of mafic rocks under pressure

J. MAUMUS, N. BAGDASSAROV,* and H. SCHMELING

Arbeitsbereich Geophysik, J. W. Goethe Universität-Frankfurt, Feldbergstraße 47, D-60323 Frankfurt am Main, Germany

(Received July 29, 2004; accepted in revised form May 16, 2005)

Abstract—We demonstrate the importance of electric conductivity measurements of partially molten mafic rocks by examining of Oman gabbro, Karelia olivinite, Ronda and Spitzbergen peridotites. The electrical conductivities of these rocks were estimated using the impedance spectroscopy at temperatures between 800°C and 1450°C and at pressures between 0.3 and 2 GPa in experiments performed in a piston cylinder apparatus. At temperatures below and above melting, samples were equilibrated during durations on the order of 200 h. Our results show that a jump in electrical conductivity can be correlated with the temperature range slightly above the solidus, due to the delayed formation of an interconnected melt phase. Thin sections of quenched samples were used to estimate volume fractions and chemical compositions of the partial melts. The increase of the electrical conductivity compares well with the connectivity of melt in partially molten samples. Above the solidus, the electrical conductivity increases by ~1 to 2 orders of magnitude in comparison with the conductivity of non-melted rock below solidus. When a complete melt connectivity is established, the charge transport follows the network of the formed melt films at grain boundaries. Durations of up to ≈200 h are required in order to reach a steady state electrical resistance in a partially molten rock sample. The experimental results were compared with the conductivity data obtained from magnetotelluric (MT) and electromagnetic (EM) measurements in the Northern part of the mid-Atlantic ridge where a series of axial magma chambers (AMC) are presumably located. There is good agreement between the measured electric conductivity of gabbroic samples with a melt fraction of 10 to 13 vol.% and the conductivity estimated at AMC, beneath the central part of Reykjanes ridge, as well as between the conductivity of partially molten peridotites and the source zone beneath the mid-Atlantic ridge at ≈60 km. *Copyright © 2005 Elsevier Ltd*

1. INTRODUCTION

The electric properties of partially molten peridotite rocks are thought to affect the depth profile of the electric conductivity in the lower lithosphere and upper mantle. Recently, a growing number of electromagnetic field experiments have constrained the electrical structure of the Earth's interior, particularly in mid-oceanic regions (Sinha et al., 1997, 1998). Based on MT and EM data, two types of electric conductivity anomalies in the Earth's crust and the upper mantle may be distinguished: high conductivity zones (HCZ) and low conductivity zones (LCZ). The combination of MT, EM and seismic studies has suggested that the partial melting of peridotites and gabbro may explain the origin of the high conductivity zones and axial magma chambers beneath the mid-Atlantic ridge (Sinha et al., 1997, 1998). The interpretations of these field data however, were not constrained by either laboratory experiments or theoretical models of partial melting, which can be important in determining what and where is the melting and how it extends beneath mid-oceanic ridges and other tectonic environments where partial melting presumably occurs. Thus, a direct comparison between laboratory measurements and field observations of the electrical conductivity of crust and upper mantle is a vital need for a more robust interpretation of field geophysical data.

One of the fundamental physical properties of rocks which can be successfully measured in field and laboratory, is the

electrical conductivity σ . The resistance R of a sample depends on its geometry and a specific resistance of rock under test ρ . For a homogeneous sample of area A and a length L , having a parallel plate geometry, it follows

$$R = \rho \frac{L}{A} \quad (1)$$

The reciprocal value of the specific resistance is called specific conductivity σ :

$$\sigma = \frac{1}{\rho} \quad (2)$$

Most rock forming minerals in the upper mantle and lithosphere are ionic or electronic conductors. Ionic conductivity relates to the diffusion transport process of charge carriers in bulk of minerals and on the grain boundaries via a diffusion coefficient of the charged species and the relation

$$\sigma = \frac{Dz^2e^2n}{kT} \quad (3)$$

which is a form of the Nernst-Einstein equation where D is the diffusion coefficient, z the valence of conducting species, e the charge of electron, n is the concentration of the conducting species, k is the Boltzmann constant and T the absolute temperature in Kelvin. In olivine, for example, the contribution from ionic conductivity from Mg vacancies increases with temperature and exceeds the contribution from electron-polaron conduction mechanism at $T > 1150^\circ\text{C}$, which is the dominant electric charge transport mechanism at lower temper-

* Author to whom correspondence should be addressed (nickbagd@geophysik.uni-frankfurt.de).

Present address: Laboratoire Magmas et Volcans, Université Blaise Pascal, 5 rue Kessler, 63038 Clermont-Ferrand cedex, France.

atures. Several works have addressed the question at which conditions differing temperature and fO_2 dependencies of σ , i.e. ionic and electronic conduction mechanisms, operate in olivine (see Constable and Roberts, 1997; Hirsch et al., 1993; Hirsch and Shankland, 1993; Sakamoto et al., 2002; and references therein). The question which still remains open concerns the charge carriers that predominate in the overall electrical conductivity in minerals composing peridotitic rocks. The mechanism of a charge carrier transport can be discriminated through measurement of the Seebeck coefficient or thermopower, i.e. the voltage generated across a sample in a thermal gradient (e.g. Schock et al., 1989), or from the temperature dependence of electrical conductivity $\sigma(T)$ in Eqn. 3 and its activation energy E_a , derived from the Arrhenius dependence of σ . The electrical conductivity measurements should be done in this case in a wide range of frequencies ω and temperatures T .

The impedance spectroscopy method in application to electrical conductivity of rocks consists of measuring the R - C parameters of equivalent circuits as a function of T and P at varying frequency ν or cycle-frequency $\omega = 2 \cdot \pi \cdot \nu$. The measured complex electric impedance which consists of real $Z'(\omega)$ and imaginary components $Z''(\omega)$ may be presented in an Argand plot, a graph of $-Z''(\omega)$ vs. $Z'(\omega)$. In a parametric form, the total electric impedance $Z(\omega)$ may be described as a sum of two or more terms as follows

$$Z(\omega) = \frac{R_1}{1 + (j \cdot \omega \cdot \tau_1)^{\alpha_1}} + \frac{R_2}{1 + (j \cdot \omega \cdot \tau_2)^{\alpha_2}} + \dots \quad (4)$$

where $R_{1,2}$ is the active resistance, $\tau_{1,2}$ is the dielectric relaxation time, and $\alpha_{1,2}$ is the exponent characterizing the deviation of a particular relaxation process from a Debye type of relaxation. The first term in Eqn. 4 responsible for high frequency behavior ($>10^3$ Hz) usually refers to bulk properties of a tested sample, the second term is attributed to the grain boundary properties of constituent minerals (Macdonald, 1987) and attributed to intermediate frequency properties. A third term, which is omitted in Eqn. 4, may describe the R - C properties of electrodes or low frequency dispersion (<1 Hz). Under pressure and after a reasonable annealing time, the contribution from the grain boundary R - C term becomes negligible (Huebner and Dillenburg, 1995) in comparison with the bulk term. Thus, by fitting an observed Argand plot to Eqn. 4, the bulk properties of a rock sample, resistance R_1 , dielectric relaxation time τ_1 and a parameter of a constant phase element α_1 , can be estimated. From experiments conducted at varying T , the temperature dependence of $R_1(T)$, $\tau_1(T)$ or $\sigma(T)$ may be determined which usually follows an Arrhenius equation with the temperature independent activation energy E_a

$$\sigma = \sigma_0 \exp\left(\frac{-E_a}{kT}\right) \quad (5)$$

The use of impedance spectroscopy (AC -measurements in a wide frequency range) in measurements of natural rock samples is necessary for several reasons: (1) The conductivity of polycrystalline materials is always frequency dependent. (2) Grain interior and grain boundary conductivities operate at differing frequency ranges, but can overlap in an impedance spectrum. (3) By doing experiments over a wide range of

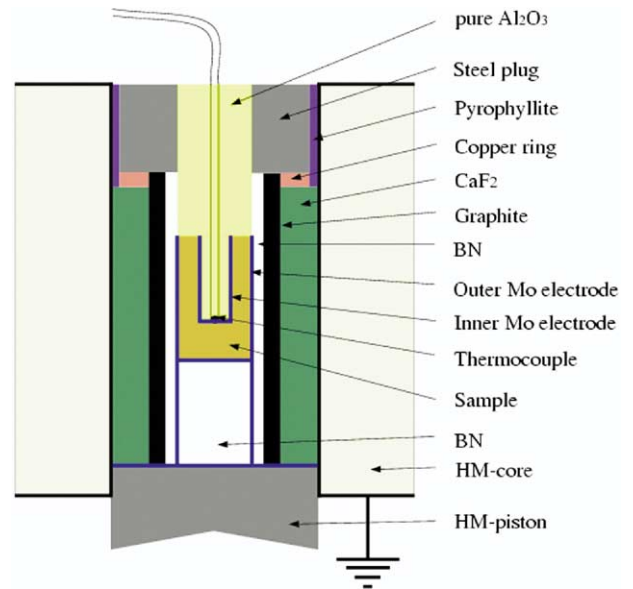


Fig. 1. Design of the coil assembly (not to scale). Outer diameter 0.5 inch.

temperatures, contributions from differing charge transport mechanisms corresponding to differing frequency ranges can be identified.

The measured complex impedance is characterized by two components $Z'(\omega)$ and $Z''(\omega)$. Impedance spectroscopy (IS) involves the measurement of Z' and Z'' as a function of ω in a large frequency range. Until now, only a few experimental works have been performed to measure the electrical conductivity of partially molten peridotite rocks at lower crust or upper mantle conditions. The experiments were mainly conducted on partially molten rocks at atmospheric pressure (Partzsch, 1997; Roberts and Tyburczy, 1999). Despite the fact that the electric conductivity of rocks at HP/HT depends weakly on pressure, the effect of pressure in the case of partially molten rocks is important because the solidus temperature directly depends on pressure. In this work *in-situ* partial melting of mafic and ultramafic rocks was monitored by the use of electrical conductivity at crustal and upper mantle P - T conditions.

For monitoring of the variations of electrical conductivity in a piston cylinder over very long durations a special construction of a measuring cell was developed and tested. The measuring cell has been used in a form of a concentric cylinder capacitor (Fig. 1). This cell was calibrated by using several standard materials (boron nitride, Al_2O_3 , NaCl, CsCl etc.). With the use of this cell the electrical conductivity of natural and analog rocks under pressures up to 2 GPa has been investigated. The temperature of experiments varied from 800°C to 1470°C. With the help of this measuring cell the partial-melting of some peridotites and oceanic gabbro was characterized via the electric measurements. During an experiment, when a rock sample starts to melt, the occurrence of the first percentage of melt can be detected by an abrupt decrease of the electrical resistance. Time variations of the melt fraction and melt topology during progressive melting produce a direct effect on the electrical conductivity of the rock sample. After melting, the quenched samples were examined, and the melt distribution

and the melt volume fraction were characterized in order to find a quantitative relationship between molten rock textures and electrical conductivity. Finally, the electrical conductivity measurements are compared with field electromagnetic measurements in order to answer the question: Do the electrical measurements realized in laboratory on molten rock help petrologists and geophysicists to better constrain the data obtained from deep Earth probing?

2. DESCRIPTION OF EXPERIMENTS

2.1. Measuring Cell for Electrical Conductivity

The pressure experiments were performed in a conventional 0.5-inch end-loaded piston-cylinder apparatus. The construction of the measuring cell is described elsewhere (Khitrov et al., 1970; Bagdassarov et al., 2001) and presented in Figure 1. The cell assembly consists of a sleeve of CaF₂, as a pressure transmitting media, a sleeve of graphite as a furnace, a sleeve of boron nitride to insulate sample from furnace. The sample is located in the center of the cell assembly. In all experiments, the pressure was increased manually with a hydraulic pump up to the desired pressure, then an automatic motorized hydraulic pump was switched on to maintain a constant oil pressure. The pressure calibration of the cell was established using several standards. The room temperature calibration has been performed by using the phase transitions in bismuth: BiI – BiII at 2.56 GPa and BiII – BiIII at 2.7 GPa (Bean, 1983). Standard points for high temperature calibrations were melting curves of NaCl and CsCl (Bohlen, 1984) and α - β transition in LiNaSO₄ (Bagdassarov et al., 2001). The melting points of NaCl and CsCl as a function of pressure were estimated from *in-situ* electrical conductivity measurements at a fixed electrical frequency of 1 kHz. A jump of conductivity of ~ 2 orders of magnitude indicated the melting point of chlorites. The accuracy of the pressure calibration is ± 0.03 GPa. The temperature gradient in the cell was estimated with the use of Al₂O₃ powder instead of a sample and by placing three S-type thermocouples located in three different points close to the middle of the graphite furnace (see Fig. 1). The radial temperature gradient is $\approx 1^\circ\text{C}/\text{mm}$. The axial temperature gradient was estimated to $\approx 2^\circ\text{C}/\text{mm}$ in the temperature range up to 900°C, $\approx 5^\circ\text{C}/\text{mm}$ between 900°C and 1200°C, and increases up to $\approx 12^\circ\text{C}/\text{mm}$ at 1500°C. This design of the measuring cell has been successfully used in previous studies of phase transitions in calcite (Bagdassarov and Slutskii, 2003) and in quartz (Bagdassarov and Delépine, 2004). The sample rock powder was placed between two metallic coaxial cylindrical electrodes made of Mo-foil (thickness 0.5 mm) having inner and outer diameters 2.1 and 3.9 mm, respectively. Thus, the radial sample thickness is 0.9 mm. The choice of Mo instead of traditional Pt-foil as an electrode material was dictated by the necessity to prevent the loss of Fe from a sample into the electrodes. The outer electrode was in contact with the boron nitride (BN) sleeve and the inner electrode is wrapped around a Al₂O₃-ceramic straw 2 mm in diameter. The alumina ceramics has two to four inner capillars for thermocouple wires. In most experiments S-type and B-type thermocouples were used to monitor the temperature. The thermocouple junction is located at the end of the Al₂O₃ ceramic in electrical contact with the inner electrode. B-type thermocouples (Pt-30%Rh/Pt-6%Rh) are more stable at high temperatures ($T > 1200^\circ\text{C}$ with an accuracy of 0.5% $> 800^\circ\text{C}$). To avoid the contamination of a thermocouple junction from a sample material, the open end of the inner electrode was sealed with a Mo-foil disk preventing contact between sample and Al₂O₃ ceramics. The sample length varies from 4 to 5.5 mm. The rest of the space in the inner BN-sleeve between the sample and the hard metal (HM) piston was filled with a BN-ceramic plug.

The geometry of electrodes consisted of two cylindrical surfaces and one closed with Mo-foil disk end. This electrode geometry results in a more complicated geometric factor than in the case of a standard co-axial cylindrical capacitor. The correction of G_f of electrodes has been taken into account to calculate the bulk resistance of the sample. For electrodes in a form of a standard coaxial cylindrical capacitor having an outer diameter D , inner d and length L ,

$$G_{f_{\text{cylindrical}}} = \frac{2\pi L}{\ln\left(\frac{D}{d}\right)} \quad (6)$$

with a typical values of D , d and L in Eqn. 6 provides $G_f \sim 5$ to 7 cm. The application of coaxial-cylindrical electrodes results in a better measurement precision at low temperatures. For the same sample volume: $G_{f_{\text{parallel-plate}}} \leq G_{f_{\text{cylindrical}}}$, which means that the measured sample resistance is smaller in the case of a concentric cylinder than in the case of a parallel plate capacitor. Thus, the ratio of the shunt resistance to the sample resistance is larger in the case of a co-axial capacitor. In addition, the outer cylindrical electrode plays a role of electric shield against electrical noise produced by the graphite heater operating at 50 Hz and at voltages up to 12 V. By the use of co-axial cylindrical electrodes, the vertical electrode axis is parallel to the piston motion, and the electrode corrugation during pressurization of a sample is minimized. The changes of the cell geometry measured after the high pressure experiments for $L_{\text{inner-electrode}}$ and D are 3% to 4% and 1% to 2%, respectively. These sample and electrode deformations do not significantly affect the results of electrical conductivity measurements. A small deviation of the cell geometry from a co-axial cylindrical geometry (see Fig. 1) is due to the inner electrode having a shorter length than the outer electrode and an additional surface at its closed end. The deviation of G_f from $G_{f_{\text{cylindrical}}}$ has been estimated from calibration measurements by using aqueous NaCl solutions of varying molality at atmospheric pressure and temperature. The conductivity of aqueous NaCl solutions were measured in a cell identical to the cell used in high pressure experiments and were compared with the table values (Carmichael, 1982). The correction factor of $\sim 25\%$ has been introduced into the final calculation of the geometric factor G_f in Eqn. 6.

A Solartron 1260 (Schlumberger Co.), frequency gain-phase analyzer was used for the impedance spectroscopy measurements. The instrument is equipped with Novocontrol software package, which provides measurements of electric impedance over a wide range of frequencies from 10^{-3} to $32 \cdot 10^6$ Hz with a maximum resolution of 10^{-3} Hz and an error of 100 ppm in phase estimations. During the measurements, the ground of the piston-cylinder press was isolated from the ground of Solartron, and the measurements were realized in a “free-ground” configuration. One wire of the thermocouple and the mass of the high pressure autoclave were used to connect inner and outer electrodes to the input and output of the gain-phase analyser. Before starting a piston-cylinder run, the cell (Mo-electrodes without sample) and connecting wires were calibrated for short (space between electrodes was filled with a copper sleeve) and open (space between electrodes was empty) circuits in the frequency range 1 MHz to 0.01 Hz. The AC-resistance of the cell in short circuit was typically $\approx 0.4 \Omega$. A complete description of the impedance spectroscopy method (IS) can be found in Macdonald (1987).

2.2. Sample Description

Natural rock samples used in this study were from the oceanic crust and the upper mantle, gabbro and peridotites. A synthetic rock sample prepared from a mixture of olivine and a synthetic basalt was also used in experiments to model melting with a known melt percentage. After experiments, samples were quenched, cut perpendicular to the electrode axis, mounted in epoxy and polished for electron probe micro-analysis (EPMA) to provide sample texture images. Rock samples were prepared by crushing chips of natural rocks. After grinding in the agate mortar, mineral grains had a maximum size of 40 to 50 μm that is much smaller than the gap between two electrodes (0.9 mm).

For sintering of a synthetic rock compact (synthetic basalt + San Carlos olivine), the synthetic basalt was prepared from high purity oxides (Chempur Co.) and carbonates grounded into fine powder under acetone. The powder mixtures were dried at 150°C and then fired during 10 h at 1000°C in a CO₂/H₂ atmospheric furnace with gas flow rates adjusted to yield an oxygen fugacity between magnetite-wüstite and iron-wüstite buffers ($f_{\text{O}_2} = 10^{-15.9}$ Pa). The resulting glass was crushed and ground to a grain size of ~ 5 to 10 μm . San Carlos olivine grains were ground to a 25- μm maximal grain size. The uniform grain size in powder compacts was provided by sorting mineral grains in a

Table 1. Chemical composition of Oman gabbro in wt.%.^a

Oxides (wt.%)	Cpx	Opx	Plg
SiO ₂	52.77	54.28	46.17
Al ₂ O ₃	2.04	1.17	34.23
FeO (total)	7.59	15.76	0.56
CaO	20.96	1.34	17.40
MgO	15.74	26.83	0.06
MnO	0.21	0.37	0.01
Na ₂ O	0.28	0.03	1.54
TiO ₂	0.35	0.18	—
Cr ₂ O ₃	0.05	0.02	0.02
NiO	0.02	0.03	—
P ₂ O ₅	0.01	—	—

^a Average microprobe analysis on 5 to 7 grains.

vertical Erlenmeyer using a selective sedimentation of grains in water. Olivine and basalt were mixed together under ethanol and evaporated in order to produce a homogeneous fine powder in the proportion 95 to 5 wt.%.

Before cell preparation, all sample powders were kept 24 h in a dryer at 150°C. After drying, powders were pressed into the cylindrical gap formed by outer and inner electrodes of a measuring cell (Fig. 1). Powders were compacted and pressed with special tools, and then pressurized in a piston-cylinder.

Two crustal rocks were investigated, an oceanic gabbro rock sample from Oman ophiolites and a continental olivinite sample from the layered intrusion in Karelia, Russia. The Oman gabbro sample is a gabbro containing 46 vol.% plagioclase feldspar, 40% orthopyroxene (Opx) and 14% clinopyroxene (Cpx). Its complete chemical composition is presented in Table 1. Oman ophiolites are interpreted as a material of an ancient oceanic ridge obducted on Arabic plate platform with a relatively small deformation. Probably, Oman ophiolites formed at a fast spreading ridge and differ from the crust formed at a slower spreading ridge (Nicolas, 1989). This gabbro sample represents a cumulate gabbro formed by partial crystallization of a melt, from which the residual melt fraction has been removed. The formation of this 2-pyroxene gabbro has been discussed in the literature and is interpreted as a result of the successive intrusions from a perched magma lens (Henstock et al., 1993), or by crystallization along the floor of the magma lens with a subsequent subsidence, or perhaps a combination of these two mechanisms (Boudier, 1996). In any case, this gabbro composition is representative of the lower crustal rocks formed in magma chambers at a mid oceanic ridge axis.

The Karelia olivinite sample stems from the large intrusive massif Kivakka-Olanga (North Karelia, Russia). It is a product of high temperature differentiation and crystallization of a magmatic pluton. This pluton was a long lived magma chamber that developed above a local mantle plume whose origin is associated with the activity of the megaplume responsible for the formation of Baltic shield province (Chistiakov et al., 2002). The age of the pluton is 2.42 to 2.44 Ga estimated from Sm-Nd and U-Pb methods (Koptev-Dvornikov et al., 2000). The sample represents an olivinite cumulate layer with low Mg number in olivine crystals, ~Fo₈₂₋₈₄. Karelia olivinite is composed of 76 vol.% Ol, 3% Cpx, 7% Opx and 14% of plagioclase feldspar (chemical composition is listed in Table 2).

Two natural lherzolite samples, from Ronda (Spain) and from Spitzbergen (Norway), representative of the upper mantle were also chosen for electrical conductivity measurements. The Spitzbergen sample represents an “anhydrous” spinel lherzolite from a peridotite xenolith uplifted in the nepheline basanite environment during Pleistocene from the upper mantle through a relatively thick continental crust and found in the Sverre volcanic center, NW of Spitzbergen. A summary of the tectonic setting can be found in Admunsen et al. (1987). The rock is composed of 68 vol.% Ol, 22% Opx, 8% Cpx and 2% Spl. Mineral compositions are presented in Table 3. The Ronda peridotite belongs to a large sub-continental peridotite massif located in Betic-Rif chains of SW Spain, which is known to have preserved peridotite metamorphic facies. It was emplaced during orogeny in Betic-Rif realm. The general feature of the massif is presented in Obata (1980) and van der Wall and

Table 2. Chemical composition of Karelia olivinite in wt.%.^a

Oxides (wt.%)	Ol	Opx	Cpx	Plg
SiO ₂	39.15	51.06	51.17	55.67
Al ₂ O ₃	0.02	6.47	3.25	26.82
FeO (total)	14.97	6.08	5.09	0.01
CaO	0.05	0.35	20.04	9.91
MgO	44.07	32.03	16.05	0.04
MnO	0.22	0.15	0.14	0.01
Na ₂ O	0.01	0.05	0.61	5.80
TiO ₂	0.02	0.08	0.49	0.07
Cr ₂ O ₃	0.01	1.76	0.93	0.02
NiO	0.32	0.08	0.04	0.01
K ₂ O	—	—	—	0.28
P ₂ O ₅	0.01	—	0.01	0.03

^a Average microprobe analysis on 5 to 7 grains.

Vissers (1996). The sample which has been measured is a spinel lherzolite composed of 68 vol.% Ol, 25% Opx, 6% Cpx and 1% Spl. Its chemical composition is presented in Table 4. Some traces of serpentine were detected in the sample (<1%), they believed do not affect the electrical conductivity and melting point of the rock.

The compact powder aggregate consisting of the San Carlos olivine and synthetic basaltic glass has been used as an analog of a partially molten rock representing a source of the magma beneath a mid-oceanic ridge. The content of the basalt glass recovered from the sample after HP-HT experiments was ≈4.5 vol.%. Chemical compositions of the olivine and basalt glass are presented in Table 5. This particular basalt composition has been calculated according to Ghiorso and Sack (1995) in order to be close to the equilibrium with San Carlos olivine crystals during a long sintering process of a powder compact.

3. RESULTS OF MEASUREMENTS

For all samples, the experimental procedure was as follows:

1. Samples were first pressurized to 0.3 GPa and heated up to 400°C and kept at this temperature for 24 h.
2. Samples were heated to a temperature 900°C to 1000°C with a heating rate of 20°C/h to 25°C/h and kept for 24 h in order to obtain well sintered samples.
3. Samples were cooled to a temperature of 800°C and kept at this temperature until we reached a stable value of the electrical conductivity which takes ~200 h.
4. Then, electrical measurements started: the temperature was increased stepwise only if a constant electrical conductivity was observed during the preceding 12 to 24 h (the temperature step varied between 10°C and 50°C). Larger steps

Table 3. Chemical composition of Spitzbergen lherzolite in wt.%.^a

Oxides (wt.%)	Ol	Opx	Cpx	Spl
SiO ₂	40.24	55.16	52.11	0.04
Al ₂ O ₃	0.01	3.07	5.23	52.30
FeO (total)	8.80	5.65	2.14	10.66
CaO	0.03	0.39	21.02	—
MgO	48.68	33.10	14.86	19.24
MnO	0.13	0.15	0.08	0.12
Na ₂ O	0.01	0.06	1.52	0.02
TiO ₂	0.01	0.07	0.35	0.05
Cr ₂ O ₃	0.01	0.34	1.01	16.27
NiO	0.37	0.08	0.04	0.31
P ₂ O ₅	0.01	—	0.01	—

^a Average microprobe analysis on 5 to 7 grains.

Table 4. Composition of Ronda lherzolite sample in wt.%.^a

Oxides (wt.%)	OI	Opx	Cpx	Spl
SiO ₂	41.11	54.65	53.11	0.03
Al ₂ O ₃	0.01	4.69	5.36	50.83
FeO (total)	8.54	5.61	2.16	12.10
CaO	0.02	0.96	21.61	—
MgO	51.44	33.97	15.89	19.67
MnO	0.13	0.14	0.08	0.13
Na ₂ O	0.01	0.05	1.26	—
TiO ₂	0.01	0.05	0.11	—
Cr ₂ O ₃	0.01	0.72	1.16	17.39
NiO	0.41	0.08	0.03	0.27
P ₂ O ₅	0.02	0.01	0.02	—

^a Average microprobe analysis on 5 to 7 grains.

were taken when the temperature was far from the expected solidus temperature. After each temperature step, IS measurements were performed every 15 to 60 min, and the electrical conductivity was estimated from the fitting of an equivalent circuit composed of two R-CPE elements connected in series according to Eqn. 4 to the experimental complex impedance. Using this heating procedure, we were not able to maintain a fixed heating rate. Samples required more time to reach a stable electrical conductivity at low temperatures compared to higher temperatures. For each temperature, the last conductivity measurement was kept as a final value and plotted in an Arrhenius plot ($\log[\sigma]$ vs. reciprocal temperature $1/T$, K).

- In some cases, as temperature was increased stepwise the measured conductivity did not correspond to the expected extrapolation of the linear Arrhenius plot defined by the previous measurements (step 4). If the measured electrical conductivity exceeded the extrapolation of the linear Arrhenius plot, then this temperature was considered corresponding to the occurrence of melt interconnection in the sample. When melt becomes interconnected through the sample, a conductivity jump is observed and the procedure continued with step 6.
- When a significant conductivity increase was observed, temperature was kept as constant and the sample electrical

Table 5. Composition of San Carlos olivine and synthetic basalt glass in wt.%.^a

Oxides (wt.%)	OI (95%)	Synthetic basalt glass (5%)
SiO ₂	40.86	45.33
Al ₂ O ₃	—	11.73
FeO (total)	9.53	9.20
CaO	0.06	10.36
MgO	50.07	12.96
MnO	—	0.17
Na ₂ O	—	2.31
TiO ₂	—	0.78
Cr ₂ O ₃	—	2.32
NiO	—	0.05
P ₂ O ₅	—	0.10
K ₂ O	—	0.33

^a Average microprobe analysis on 5 to 7 grains.

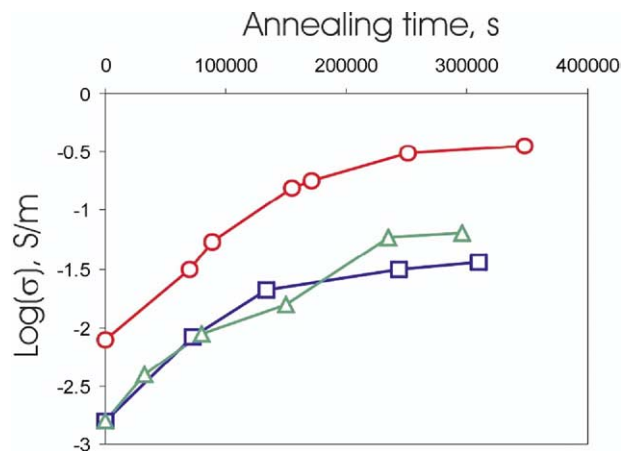


Fig. 2. Variation of electrical conductivity with time for Oman gabbro samples at 1 GPa and 1240°C (circles), 0.5 GPa and 1188°C (squares) and 0.3 GPa and 1196°C (triangles). The large increase of conductivity is attributed to development of a connected network of melt within the samples.

conductivity was measured until it reached a steady state value (a duration of 2–5 d) at that temperature (see Fig. 2).

- The sample was quenched in order to “freeze” the partially molten textures. Pressure was slowly returned to 0.1 MPa and the sample was prepared for the observation of melt distribution.

At temperatures $< 800^\circ\text{C}$ it was not possible to perform a reliable electrical measurement in the desired frequency range (10^{-2} – 10^5 Hz), as the apparent resistance of the sample was too high and the quality of the impedance spectra was substantially reduced. Several factors may account for the observed disturbances of the electrical signal and poor quality of the Argand plots: (1) at low frequencies the quality of the electrical contact between a sample and electrodes is not perfect; (2) the electrical noise is produced by the graphite furnace, which interferes with the signal and decreases the resolution of a phase delay of Solartron. With the temperature increase the applied to the graphite heater electrical current (~ 300 – 350 A) produces a voltage noise which becomes comparable and even larger than the electrical signal generated by Solartron (1–1.5 V); (3) the capacitance of the electrode-sample interface may hide the capacitance of the sample; (4) the sample conductivity at low temperatures cannot be measured because of the smaller ratio between shunt and sample resistances.

At temperatures $> 800^\circ\text{C}$ IS measurements were performed in a frequency range of 10^{-2} to $5 \cdot 10^5$ Hz. When the melting temperature was reached no significant changes in the shape of the impedance spectra were observed (see example of Oman gabbro in Fig. 3). Below the solidus, the impedance spectra are similar to those reported by Roberts and Tyburczy (1991, 1993) for their polycrystalline compacts and also similar to the results of Huebner and Dillenburg (1995); (1) a semi circle at high frequencies (HFC), which is related to the bulk grain impedance; (2) and only a portion of a semi-circle at low frequencies (LFC) that may be attributed to electrode-sample interface (left and right hand sides of Fig. 4, respectively). At intermediate frequencies, a contribution from a grain boundary impedance could be expected but it is not observed, likely due to well

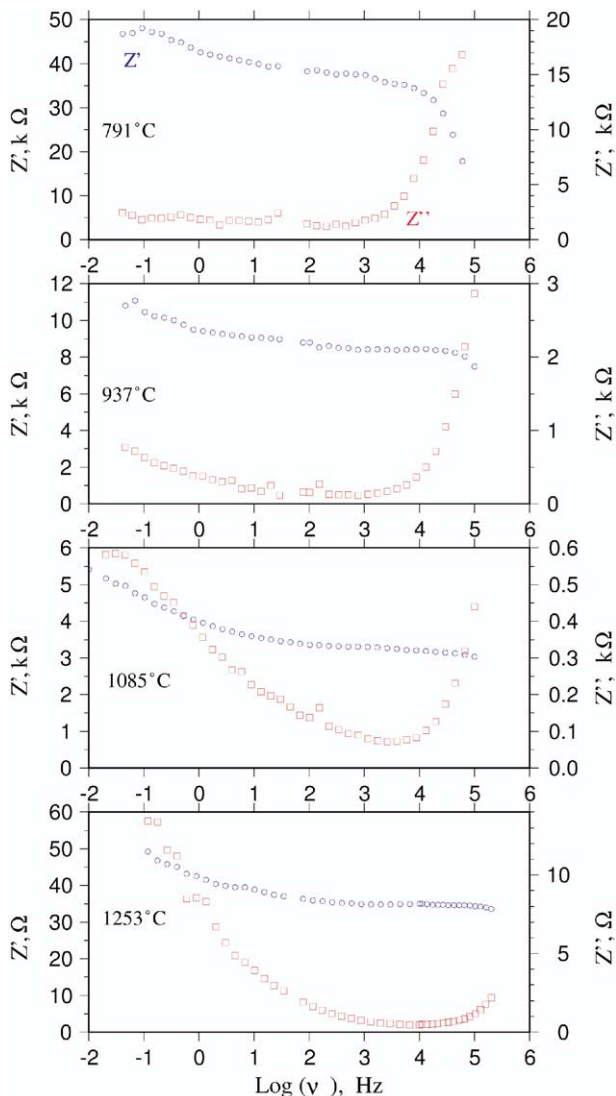


Fig. 3. Impedance spectrum of Oman gabbro sample at 791, 931, 1035 and 1253°C at 1 GPa. For each temperature, $\text{Re}(Z)$ and $\text{Im}(Z)$ vs. $\log(\nu)$ are represented by circles and squares, respectively.

sintered of grain boundaries under pressure long annealing times. With increasing temperature, the general shape of the impedance spectrum remains semi-circular but the diameter of the semi-circle decreases. This is due to the increase of the bulk conductivity. At high temperatures, the HFC maximum and intersection (or cusp in Fig. 4) with the horizontal axis, is progressively shifted to higher frequencies, and the spectrum does not display a complete semi-circle but rather a small portion of this semi-circle. Thus, the contribution from the electrode-sample interface becomes more significant at high temperatures and shifts to high frequencies. At maximum temperatures of experiments $\sim 1250^\circ\text{C}$ the typical frequencies of the cusp in Figure 4 is $\sim 2\text{--}3 \cdot 10^3$ Hz. At temperatures above the solidus, no significant changes in the shape of spectra are observed in comparison with impedance spectra below the solidus. This could indicate that the presence of melt at grain boundaries decreases further the grain boundary resistance and

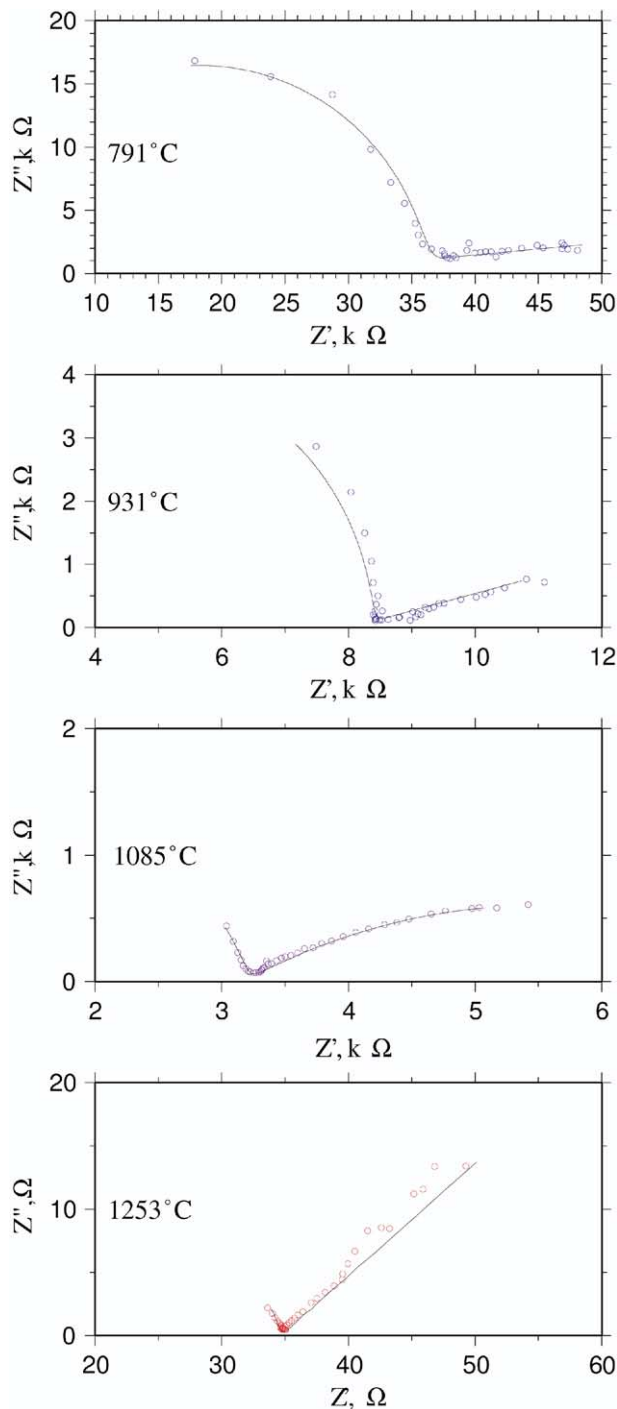


Fig. 4. Examples of Argand diagram for Oman gabbro at 1 GPa. The corresponding impedance spectrum is presented in Figure 3.

shifts a hidden grain boundary semi-circle into the high frequency range. In Figures 3 and 4 at 791°C , 931°C and 1085°C , the estimated conductivity is associated with a melt-free rock electrical conductivity. At 1253°C , the lowest value of the sample resistance and the highest value of conductivity correspond to the presence of melt in the sample. At subsolidus temperatures, the sample conductivity displays a linear increase with reciprocal temperature that can be fitted by an Arrhenius

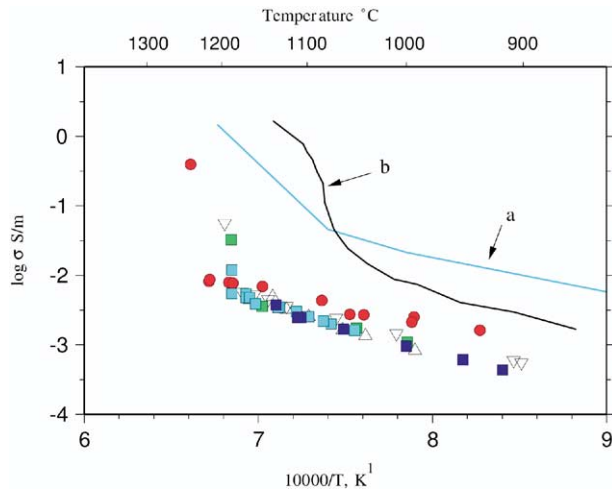


Fig. 5. Electrical conductivity of Oman gabbro sample at 0.3 (triangles), 0.5 (squares) and 1 GPa (circles) pressure: for each sample, above solidus, the samples display a behavior that can be fitted the Arrhenius dependence $\sigma = \sigma_0 \exp(-E_a/kT)$. A general fit of data provide $E_a = 1.38$ eV and $\log \sigma_0 = 2.51$ S/m. Note the dramatic jump of conductivity at 1240, 1188 and 1196°C for 1, 0.5 and 0.3 GPa experiments respectively. Measurements on olivine gabbros of (a) Sato and Ida (1984); (b) Partzsch (1997), Schilling et al. (1997), and Partzsch et al. (2000) are shown for comparison.

equation (Eqn. 5). The activation energy corresponding to the bulk conductivity mechanism can be estimated from the slope of the equation (see Fig. 5). Above the solidus, when a jump in conductivity is detected, temperature was kept constant and the impedance spectra were measured as a function of annealing time in order to observe the time variation of conductivity. The presence of melt implies an important change in the conductivity of a rock due to the contrast between the conductivities of the rock grain interior and that of the melt, which is ~ 2 to 3 orders of magnitude higher. Thus, the partial melting of a rock has been detected from electrical impedance.

The melt occurrence will effectively increase the overall conductivity only when the melt phase is interconnected. At small melt fractions, the melt may be partially distributed in a form of isolated pockets between mineral grains. When the melt fraction is large enough, the geometry of the melt phase becomes interconnected and the melt network controls the overall sample conductivity. Thus, the increase of the electrical conductivity at high temperatures does not correspond to the occurrence of the first percentage of melt or the onset of melting above solidus temperatures. This increase may be shifted to higher temperatures due to a delay in the establishing of an interconnected melt network. The attainment of a steady state electrical conductivity in a partially molten rock requires a long time (Fig. 2). Only after 2 to 4 d, the conductivity is observed to reach a steady-state value which is 1 to 3 orders of magnitude higher than the conductivity of melt free samples prior to melting, or containing small amounts of non-interconnected melt (Fig. 2). A gabbroic rock from Oman ophiolites was investigated at 0.3, 0.5 and 1 GPa.

The results of the electrical conductivity measurements are presented in Figure 5. For each sample two stages were observed: (1) at low temperatures, the gabbro electrical behavior

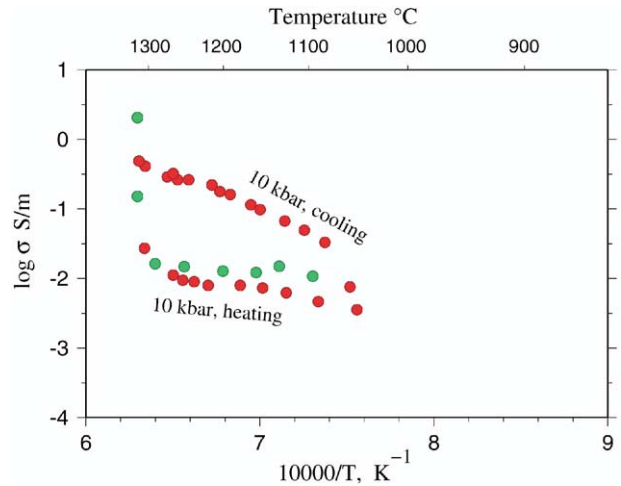


Fig. 6. Electrical conductivity of Karelia olivinite sample: two runs were performed at 1 GPa. The first run was quenched at 1315°C corresponding to the conductivity-jump temperature. The second run was cooled after 24 h with a cooling rate about 20°C/h. The parameters of the Arrhenius dependence for Karelia olivinite below solidus: $E_a = 0.82$ eV and $\sigma_0 = 0.67$ S/m.

can be fitted by an Arrhenius expression (Eqn. 4). In this pressure range, no significant variation of conductivity can be observed with pressure, and the temperature dependence may be fitted with $E_a = 1.38$ eV and $\log \sigma_0 = 2.51$ S/m. (2) At higher temperatures, the conductivity increases dramatically taking several days until it remains stable (Fig. 2). This conductivity jump is observed at 1240°C (1 GPa), 1196°C (0.5 GPa) and 1188°C (0.3 GPa), and it ~ 1 to 2 orders of magnitude. This large conductivity change is related to the occurrence of a first interconnected melt network in gabbro. At the stage of the attainment of an interconnected melt network, the melt conductivity starts to control the conductivity of gabbroic samples. The conductivity increases with time because (1) the melt reaches slowly chemical equilibrium with pyroxene grains; (2) the melt textural interconnection is delayed due to a slow migration (mechanical-equilibration) processes of the melt phase in presence of pyroxenes. The temperatures associated with the conductivity-jump are $> 50^\circ\text{C}$ higher than the expected solidus temperature of this pyroxene gabbro estimated from their viscoelastic behavior at atmospheric pressure (Bagdassarov, 2000).

Two experiments were performed at 1 GPa on Karelia olivinite samples. The general behavior of the first experiment, presented in Figure 6, is close to that observed in Oman gabbro samples. Conductivity data for the melt-free rock can be fitted by the Arrhenius equation with $E_a = 0.82$ eV and $\log \sigma_0 = 0.67$ S/m. Comparing this with the conductivity of the Oman gabbro (having $E_a = 1.38$ eV), the Karelia olivinite is more conductive, having a lower activation energy. This may be explained by compositional differences between these two rocks, as olivinite is an olivine-rich rock. The olivine crystals possess higher Fe content (Mg number is 84), and this may explain higher conductivity and lower activation energy in this sample in the high temperature range. With the increasing content of Fe in olivine the electron-polaron hopping conduction may extend

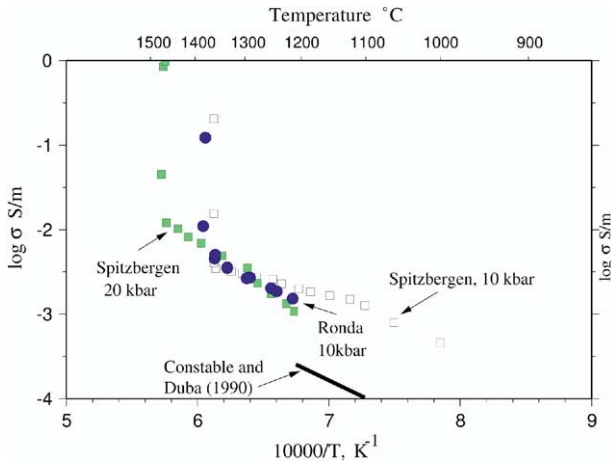


Fig. 7. Electrical conductivity of Spitzbergen (at 1 and 2 GPa) and Ronda (at 1 GPa) lherzolite samples compared with dunite (Constable and Duba, 1990). The parameters of the Arrhenius equation for melt-free rocks: Spitzbergen lherzolite: $E_a = 2.11$ eV and $\log \sigma = 4.25$ S/m; Ronda lherzolite: $E_a = 1.61$ eV and $\log \sigma = 2.65$ S/m.

to higher temperatures (Constable and Roberts, 1997; Sakamoto, 2002).

Above the solidus, the similar melt effect on the electrical conductivity is observed in olivinite as in gabbro. For the Karelia olivinite sample, the conductivity jump is ~ 2 to 2.5 orders of magnitude (in comparison with 1.5 orders of magnitude for the Oman gabbro at 1 GPa) and is observed at 1315°C. After reaching a stable conductivity, the sample was quenched. A second experiment was carried out at the same pressure but the sample was not quenched after the melt occurrence was detected. This second sample was, instead, cooled with a constant cooling rate of 20°C/h. During cooling the sample exhibits a higher conductivity than that from the earlier heating sequence. If a connected melt network exists in the sample, cooling could transform the basaltic melt into a glass, which possesses a higher conductivity than grain interiors. Thus, this experiment confirms that the abrupt jump in electrical conductivity corresponds to the formation of an interconnected melt network above the solidus. The electrical conductivity of Spitzbergen lherzolite has been measured at 1 and 2 GPa. At low temperatures, the pressure dependence of conductivity on pressure is insignificant. Conductivity of a melt-free sample at 2 GPa was fitted by the Arrhenius equation having parameters $E_a = 2.11$ eV and $\log \sigma = 4.25$ S/m that is slightly lower than Oman Gabbro conductivity. The observed jump in conductivity is ~ 1 to 2 orders of magnitude at 1360°C (1 GPa) and 1465°C (2 GPa). The results of the electrical measurements are presented in Figure 7.

The Ronda lherzolite was measured at 1 GPa. This rock sample exhibited small traces of serpentine around olivine crystals. To avoid the influence of the serpentine on the electrical measurement, the sample was kept for 24 h at 800°C. The conductivity measurements are presented in Figure 7. The comparison of the electrical conductivity variations with the sample texture demonstrated that after sintering the serpentine disappears. The Ronda lherzolite shows almost the same behavior as the Spitzbergen lherzolite. The low temperature be-

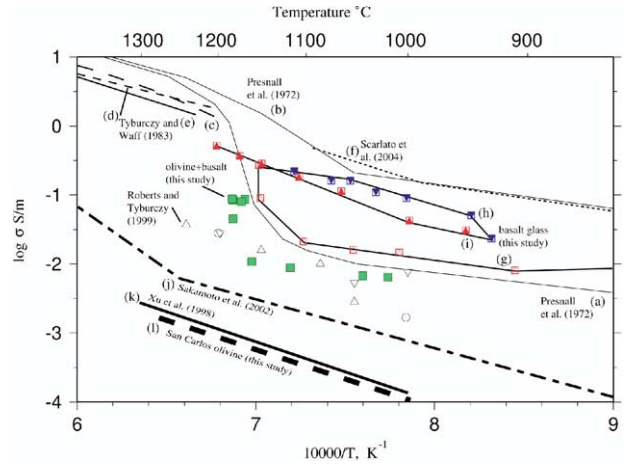


Fig. 8. Electrical conductivity of synthetic basalt glasses measured by Presnall et al. (1972) during (a) heating, and (b) cooling (thin line), tholeiitic basalt glass measured by Tyburczy and Waff (1983) at ambient pressure (c), 0.43 GPa (d) and 1.28 GPa (e), basaltic rocks measured by Scarlato et al. (2004) (f) and our synthetic olivine glass during (g) first heating, (h) cooling, (i) second heating; vs. olivine + basalt aggregates (squares, this study) at 1 GPa compared to Roberts and Tyburczy (1999) (open triangles and circles); and San Carlos olivine at 3 to 5 GPa (j) (Sakamoto et al., 2002), at 4 GPa (k) (Xu et al., 1998) and at 1 GPa (l, present study).

havior can be fitted with the Arrhenius equation ($E_a = 1.61$ eV and $\log \sigma = 2.65$ S/m). Above the solidus temperature, conductivity jump of 1 order of magnitude at 1377°C was observed.

Only one experimental work (Roberts and Tyburczy, 1999) deals with the electrical conductivity of a compact powder consisting of olivine + basalt glass, which can be compared with the studied samples of olivine + basalt aggregates (see Fig. 8). (1) In that study (Roberts and Tyburczy, 1999), Fo_{80} olivine was used, versus Fo_{90} in this study, and the basalt glass composition was different. (2) The experiments in Roberts and Tyburczy (1999) were made not directly on a starting powder mixture of olivine and basalt glass, which has been done in this study. The compact powder sample in Roberts and Tyburczy (1999) was sintered at high pressure in a piston cylinder apparatus and, then, the electrical conductivity of a sintered sample was measured in an atmospheric pressure furnace under a controlled oxygen fugacity. Thus, in the experiments of Roberts and Tyburczy (1999) it was not possible to observe the conductivity increase above solidus due to a developing melt interconnection within the sample. In Roberts and Tyburczy (1999) the increase of the electrical conductivity corresponds to the point of softening of the basalt glass, thus, the magnitude of the conductivity jump does not fully reflect the effect of melting and spreading of melt between olivine grains. The observed increase of the conductivity due to the melting in the present sample is ~ 0.5 order of magnitude higher than in Roberts and Tyburczy (1999) sample, which may be also due to the compositional differences of olivine.

A remarkable point is that the small conductivity jump was observed for a melt fraction of only 4.5 vol.% (that is, the maximum melt fraction that was allowed in this sample with a chosen basalt composition). This melt fraction is rather low

compared with the melt fraction observed in natural rock samples, gabbro, olivinite and peridotites. This is not a surprise, if one considers, that at textural equilibrium, in the system olivine + basalt melt, the basalt melt should be interconnected even at smaller melt fractions in comparison with pyroxene bearing rocks due to larger wetting angle between pyroxene crystals and melt (Zimmerman and Kohlstedt, 2004). This fact emphasizes the non-ideal wetting of melt and mineral grains in natural rocks containing more pyroxene and less olivine. In partially molten rocks containing more pyroxenes and less olivine, melt interconnection could not be reached for samples with melt fractions < 5 to 10 vol.% (Fujii et al., 1986; Toramaru and Fujii, 1986). At higher melt fractions, the interconnection of the melt occurs rapidly through the adjustment of grain boundaries adjustment to the melt phase topology.

The temperature at which the conductivity jump is detected in peridotites, is higher than the expected solidus temperature. Hirschmann (2000) compiled experiments made on natural peridotites to constraint the solidus temperature as a function of pressure. T_{solidus} may be fitted by a polynomial relationship as follows

$$T_{\text{solidus}} = a \times P^2 + b \times P + c \quad (7)$$

with T_{solidus} in °C and P in GPa. A best fit is obtained with $a = 5.104$, $b = 132.99$ and $c = 132.899$. From Eqn. 7, T_{solidus} would be 1153°C (at 1 GPa) and 1167°C (at 2 GPa) with an error of 20°C. These are significantly lower than the temperature at which partial melt affects the electrical conductivity of the Spitzbergen lherzolite.

Another experimental run was performed with the pure basalt glass compact at 1 GPa. This run was divided into three steps. (1) Sample heating: the basalt glass was heated to 1170°C where the electric conductivity increased by about one order of magnitude. (2) After keeping the melt for 12 h at 1170°C, the basaltic melt was cooled at a rate of 25°C/h. During cooling basaltic melt exhibits higher conductivity than basalt glass compact during heating. This can be explained by either a change of the sample geometry due to welding or possibly due to an irreversible change in $\text{Fe}^{3+}/\text{Fe}_{\text{tot}}$ ratio. In stage 1, the sample was a compact powder, and, thus, the conductivity is a sum of the surface and volume conduction mechanisms. In stage 2 the glass is presumably at its theoretical density at these conditions and, thus, homogeneous, and, therefore, the bulk conductivity is a dominant mechanism. (3) After keeping the sample for 12 h at 900°C, the glass was reheated up to 1240°C with a heating rate of 20°C/h. The sample demonstrated the same temperature behavior as that during stage 2. Thus, the conductivity measured during stages 2 and 3 represents the real behavior of the basaltic melt/glass. This behavior shows a good agreement with the conductivity data from Presnall et al. (1972) measured on basalt glasses. We observed that the basalt glass conductivity is 2.5 orders of magnitude higher than the conductivity of the San Carlos olivine. The electrical conductivity of the San Carlos olivine powder compact (Fig. 8) corresponds to conductivity of Ol crystals without basalt glass measured at 1 GPa, and the results are similar to those from Xu et al. (1998).

Table 6. Melt content in partially-molten quenched samples.

Sample	Quenching temperature (°C)	Melt fraction (vol.%)
Oman gabbro		
1 GPa	1240	34
0.5 GPa	1188	15
0.5 GPa	1187	12
0.5 GPa	1135	0
0.3 GPa	1196	17
0.3 GPa	1139	0
Karelia olivinite, 1 GPa	1315	10
Spitsbergen lherzolite		
2 GPa	1465	22
1 GPa	1360	14
Ronda lherzolite, 1 GPa	1377	11
Olivine + basalt sample	1183	4.5

Microprobe analysis with a beam current of 10 kV and 20 nA.

4. DISCUSSION

4.1. Product of Experiments

The samples from each experimental run were quenched, cut perpendicular to the cell axis and polished with alumina powder and colloidal silica, and prepared for the analysis of melt distribution, which was done with the use of a reflected light microscope and also from backscattered electron images obtained on the electron microprobe Jeol JXA-8900. No evidence of melt segregation on the scale of the full sample length was detected. Typically, the equilibrium distribution of melt phase is indicated by the presence of well formed triple junctions and stable melt wetted crystal faces (Waff and Bulau, 1979; Daines and Kohlstedt, 1997; Faul, 1997). This texture has been interpreted as an indication of a complete inter-connectivity of the melt (Waff and Bulau, 1979). Tables 6 to 8 list melt compositions and quench temperatures for each of the measured samples (average of 10 microprobe analyzes of glass and crystal with a beam current of 10 kV and 20 nA, and an electron beam spot of 5 μm for glass analysis). Quench temperatures correspond to those at which a detectable increase of the electrical conductivity takes place. Note that in all natural samples the partial melting was detected only for a melt fraction ≈ 10 vol.%.

The melt fraction in each sample was estimated from the image processing of SEM pictures of thin sections. The volume percentage of melt is extrapolated from the surface percentage of thin sections without correction to 3D-distribution. To be statistically representative, these estimations must be obtained from a relatively large surface of a thin section. Table 6 shows melt content and quench temperature for each measured samples, except that of the olivine + basalt sample where the melt content was fixed, and two gabbro experiments which were quenched at temperatures below the solidus. The estimated melt content is relatively high, larger than few volume percent. This is in agreement with the higher temperatures necessary to detect the effect of melt interconnectivity on the sample electrical conductivity. As it follows from the results, the electrical measurements are not sensitive enough to detect the onset of melting with a melt fraction <1% to 2%. Larger melt fractions, at least 4% to 5% are needed to detect melting via a noticeable

Table 7. Composition of melts and minerals after experimental runs at 1 GPa for Oman gabbro and Karelia olivinite samples in oxide wt.%.

Rock-sample Oxides (wt.%)	Oman Gabbro					Karelia olivinite	
	Melt	Opx1	Opx2	Cpx	Quenched-mineral	Melt	Ol
SiO ₂	50.96	56.75	55.19	53.29	49.33	43.37	40.39
Al ₂ O ₃	29.37	3.47	1.27	2.14	17.78	12.29	0.04
FeO _(total)	2.49	10.35	15.14	6.74	4.88	4.36	7.42
CaO	13.52	5.49	1.40	21.39	16.11	21.86	0.27
MgO	2.05	23.34	26.42	15.76	10.96	17.05	51.14
MnO	0.07	0.29	0.36	0.18	0.17	0.22	0.21
Na ₂ O	1.43	0.14	0.02	0.10	0.61	0.29	0.01
TiO ₂	0.06	0.15	0.18	0.36	0.14	0.32	0.01
Cr ₂ O ₃	—	0.01	0.01	0.02	0.01	0.11	0.46
NiO	—	—	0.01	—	—	0.02	0.05
K ₂ O	0.03	—	—	—	—	0.08	—
P ₂ O ₅	0.01	—	—	0.01	—	0.03	0.01

Microprobe analysis with a beam current of 10 kV and 20 nA.

increase of the electrical conductivity in olivine rich rocks. For example, in olivine + basalt compacts, where only Ol-Ol-melt triple junctions control the melt connectivity, the overall increase of electrical conductivity is moderate. In the case of pyroxene-rich samples, like pyroxene Oman gabbro, even larger melt fractions are needed to establish complete melt interconnection because of the higher pyroxene-melt dihedral angle.

Melt distribution and melt geometry are illustrated in back-scattered electrons images of quenched samples obtained by microprobe analysis. Figures 9 to 12 show examples of the melt topology. In some samples, thermal cracking during quenching correlates with the melt topology as it is shown in Figure 11. No dihedral angle measurements have been carried out, but the triple junctions appear to be larger in the Oman gabbro samples than in other samples. Different kinds of melt pockets can be detected (e.g. Fig. 10). In all samples, the melt phase or glass occurs both as an interstitial phase between olivine grains in triple junctions as well as in the form of melt pockets. The melt fraction is large in all studied samples, consequently, the melt fraction is mainly distributed in a form of large pools (see Figs. 9 and 10). We also observe some well formed and wetted triple junctions that indicates the developed melt interconnection. In

Ol-rich samples, the Ol planar faces (F-faces) control the crystal wetting (Figs. 10 and 12).

The distribution of the melt phase demonstrates the anisotropy of Ol-basalt interfacial energies. A similar melt topology is also observed in pyroxene rich samples, i.e. the formation of the non-regular triple junctions as has been described in [Cmiral et al. \(1998\)](#). In a partially molten system with an isotropic interfacial energy of mineral grains, a dihedral angle <60° implies that the melt should be interconnected at all melt fractions. In the studied samples the interfacial energy is anisotropic and this complicates the interpretation of the melt topology. If the melt fraction is low, the possibility of the occurrence of a noninterconnected melt geometry increases. Chlorine diffusion has been used as an indicator for fluid connectivity in H₂O-bearing quartzite ([Brenan, 1993](#)). Although, the H₂O-quartz dihedral angle is 57°, the results suggested a complete connectivity of a fluid phase at any volume fraction. An abrupt decrease of the bulk diffusion coefficient for chlorine between 1 and 0.3 vol.% of fluid was observed in [Brenan \(1993\)](#). This drop has been interpreted as a result of the elimination of interconnected porosity owing to the presence of a sufficient number of non-wetted grain edges. Similar results have also been obtained for the carbonate-olivine system ([Minarik and](#)

Table 8. Composition of melts and minerals after experimental runs at 1 GPa for peridotite samples and olivine-basalt compact in oxide wt.%.

Rock-sample Oxide (wt.%)	Spitzbergen			Ronda		Olivine + 5 wt.% basalt	
	Melt	Ol	Opx	Melt	Ol	Melt	Ol
SiO ₂	42.75	40.12	56.03	49.91	39.95	47.63	40.00
Al ₂ O ₃	17.90	0.35	5.07	17.40	0.13	9.89	0.15
FeO _(total)	1.56	11.02	1.12	7.21	8.38	5.24	9.86
CaO	2.14	0.36	0.16	15.09	0.29	9.37	0.24
MgO	34.51	47.68	37.20	7.76	50.77	23.48	49.07
MnO	0.25	0.21	0.10	0.15	0.14	0.14	0.15
Na ₂ O	0.16	0.05	0.01	1.79	—	1.85	0.05
TiO ₂	0.11	0.04	0.02	0.30	0.01	1.55	0.06
Cr ₂ O ₃	0.59	0.10	0.29	0.36	—	0.10	0.02
NiO	0.01	0.06	0.01	0.04	0.30	0.13	0.39
K ₂ O	0.06	0.01	—	—	0.01	0.47	—
P ₂ O ₅	—	0.01	—	—	0.01	0.16	0.02

Microprobe analysis with a beam current of 10 kV and 20 nA.

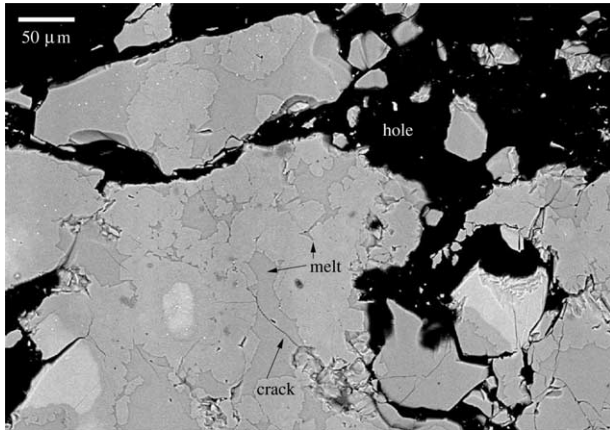


Fig. 9. Oman gabbro, 1 GPa: Backscattered electrons image (SEM) of the sample after quenching. The area is close to the outer electrode. Cracks are produced during quenching, cavities are produced during the thin section preparation. Melt is a dark gray color and crystals appear in the lightest gray color. Scale in the right upper part of picture.

Watson, 1995), in which diffusive transport of Fe into dunite as a function of a carbonate melt fraction was studied. In that study, it was concluded that melt connectivity was only established > 0.05 wt.% of melt (that is, 0.07 vol.%), despite the fact that the dihedral angle is much lower than the critical value 60° ($\approx 25^\circ\text{--}30^\circ$). In both studies, the absence of connectivity at low fluid fractions was interpreted as a result of an anisotropy of the solid-fluid interfacial energy. In other words, the differing crystallographic faces possess different interfacial energies, resulting in a differing thickness of the melt and its curvature on grain-melt interfaces depending on the crystallographic orientation of grain-faces. The connectivity threshold in the olivine-basalt system must be larger than that in the carbonate-olivine system because of the much larger dihedral angle, and

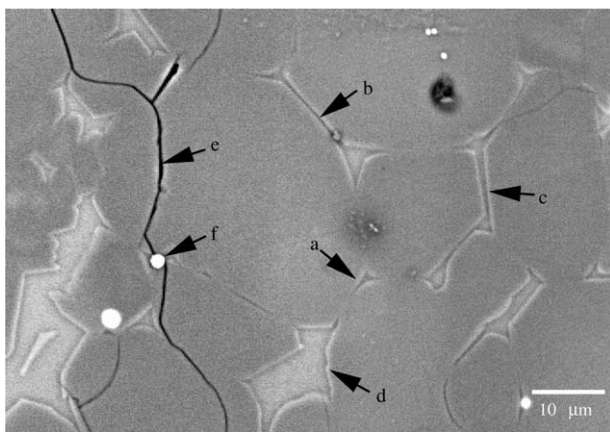


Fig. 10. Karelia olivinite, 1 GPa: SEM image of the sample after quenching. Cracks (e) are produced during quenching. This picture demonstrate different kinds of melt pockets and their shapes as described in Cmiral et al. (1998): Additionally to regular triple junctions of melt (a), we found out non-regular triple junction which are controlled by planar faces (F-faces) of olivine crystals (b, c), and larger melt pools (d). (e) Cracks developed during unloading stage. Some Fe-Ni droplets (f) indicate the low level of oxygen fugacity during experiment as expected with Mo electrodes.

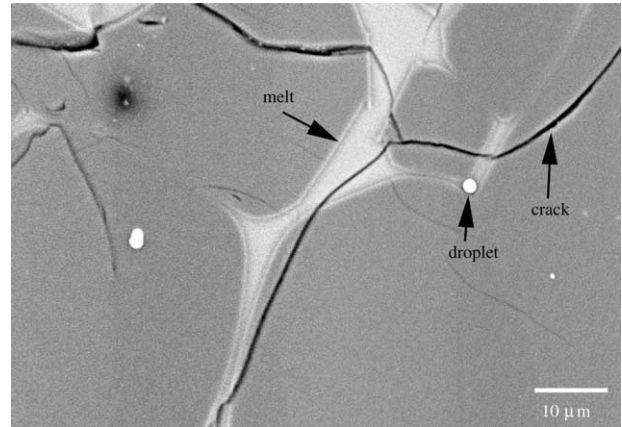


Fig. 11. Ronda peridotite, 1 GPa: Scanning electron microscope image of the sample after quenching. Cracks due to quenching intersect the melt pockets.

may be close to 0.3 vol.% as in the quartz- H_2O system. The dihedral angle is only slightly larger in this system than in the basalt-olivine system, but the degree of the interfacial energy anisotropy is more pronounced for olivine than for quartz (Laporte and Provost, 2000). Therefore, taking into account the presence of pyroxenes in most of the studied samples which probably lower the effective connectivity of the samples, it may be concluded that at low melt fractions, < 5 vol.%, a network of grain-edge channels with a low degree of connectivity can exist. This low degree of connectivity may explain the detection-limit of the melt fraction from electrical conductivity measurements.

Due to the lack of melt topology observations from our experiments, it was difficult to better discriminate between different mixing models for the electrical conductivity of partially molten samples. This is mainly due to the rather large amounts of melt present in the quenched samples. Electrical conductivity data obtained on samples with high melt fractions (10 vol.%) was used in an attempt to fit by the Hashin-

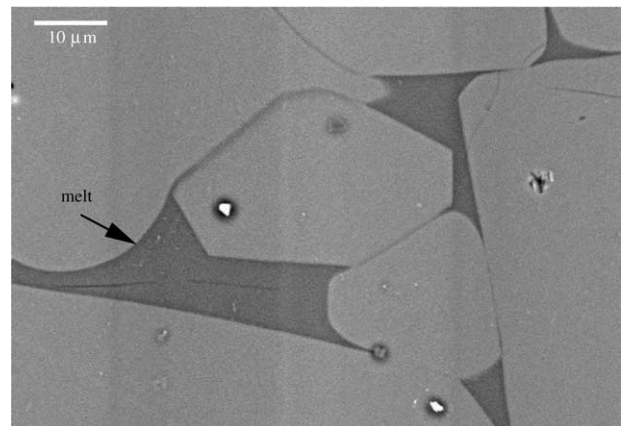


Fig. 12. Spitzbergen peridotite, 2 GPa: Scanning electron microscope image of the sample after quenching. Example of grain intersections that are controlled by a minimum the surface energy of two F-faces separated by two grains of different sizes.

Table 9. Melt conductivity needed to model the measured molten rock conductivity with Hashin-Strikman upper bound (Eqn. 8).

Sample	$T_{\text{quenching}}$ (°C)	$\log(\sigma_{\text{solid}})$ (S/m)	σ_{melt} (S/m)	X_{melt} (vol.%)	$\log(\sigma_{\text{HS}^+})$ (S/m)	$\log(\sigma_{\text{mes}})$ (S/m)
Oman gabbro						
1 GPa	1240	-2.08	1.5	34	-0.41	-0.4
0.5 GPa	1188	-2.24	0.29	15	-1.44	-1.45
0.5 GPa	1187	-2.25	0.31	12	-1.51	-1.5
0.3 GPa	1196	-2.22	0.48	17	-1.20	-1.2
Karelia olivinite, 1 GPa	1315	-1.92	28.8	10	0.30	0.3
Spitzbergen lherzolite						
2 GPa	1465	-1.86	4.9	22	-0.10	-0.1
1 GPa	1360	-2.25	2.5	14	-0.60	-0.6
Ronda lherzolite, 1 GPa	1377	-2.25	2.0	11	-0.80	-0.8
Ol + basalt sample, 1 GPa	1183	-3.06	2.9	4.5	-1.05	-1.05

Shtrikman upper bound HS^+ . This is a well known approach in the analysis of the conductivity of a composite medium consisting of two phases, otherwise known as effective medium theory (McLachlan et al., 2000). In the effective-medium model, or Maxwell-Wagner model (Maxwell, 1881; Wagner, 1914), the composite is described as a suspension of spheres dispersed in a continuous medium, and can be extended to the case of ellipsoidally shaped inclusions (Fricke, 1953). The method of Hashin and Shtrikman (1962) yields an upper conductivity bound (HS^+) and a lower conductivity bound (HS^-) and provides more realistic limits for the upper and lower limits for a composite material. HS^+ and HS^- are the possible maximum and minimum limits of the conductivity in a medium having an isotropic distribution of two phases. All models that predict a conductivity higher or lower than HS^+ and HS^- are automatically non-isotropic effective mediums. This approach provides a good estimation of a possible conductivity range for a system consisting of melt + solid grains, whether the melt is distributed as a complete interconnected network (HS^+) or in the case when the melt pockets are isolated in a solid matrix (HS^-):

$$\sigma_{\text{HS}^+} = \sigma_{\text{melt}} + X_{\text{solid}} \left(\frac{1}{\sigma_{\text{solid}} - \sigma_{\text{melt}}} + \frac{X_{\text{melt}}}{3\sigma_{\text{melt}}} \right)^{-1} \quad (8)$$

$$\sigma_{\text{HS}^-} = \sigma_{\text{solid}} + X_{\text{liquid}} \left(\frac{1}{\sigma_{\text{melt}} - \sigma_{\text{solid}}} + \frac{X_{\text{solid}}}{3\sigma_{\text{solid}}} \right)^{-1} \quad (9)$$

The results of a relative increase of electrical conductivity versus melt fraction according to the HS^+ model (Eqn. 8) are shown in Table 9.

It is clear that partial melting strongly influences bulk conductivity of rocks, but the effects of melt composition still remains unclear. Melt conductivity increases with decreasing SiO_2 content and with increasing Fe + Mg and alkali contents (Rai and Manghnani, 1977). Tyburczy and Waff (1983) show that at high temperature, ionic conduction via alkali mobility is the dominant mechanism of charge transport. They measured electrical conductivity of tholeiitic and andesitic melts, with a fixed electrical frequency of 2 kHz, at pressures up to 2.5 GPa and observed a significant decrease of the electrical conductivity (less for tholeiite than for andesite) < 1 GPa that is more pronounced at temperatures > 1200°C. Roberts and Tyburczy (1999) reported that for a Fo_{80} basalt melt system measured at 0.1 MPa, the effect of changing melt composition is balanced

by the change in temperature. A recent work on basaltic rocks from Mount Etna (Scarlato et al., 2004) demonstrate that while melts have higher conductivity due to higher alkali and Fe+Mg contents and lower SiO_2 content, the conductivity of partially molten rocks is rather more influenced by the quantity and topology of melt than to the melt composition. If we consider the high melt fractions observed in our samples, some effect of pressure or changing melt composition may be observed.

Despite the lack of a complete systematic analysis of melt chemistry vs. measured electrical conductivity, we compared the calculated melt conductivity needed to explain the conductivity jumps observed in our experiments (see Table 9) and the chemical compositions of the melts (see Tables 7 and 8). It should be noted here that (1) Peridotite samples have a rather high conductivity regarding the alkali content of the produced melts; (2) From the measurements made on Oman gabbro at 0.3, 0.5 and 1 GPa, the calculated melt conductivity increases with increasing pressure. This fact contradicts earlier results of Tyburczy and Waff (1983).

4.2. Interpretation of Field Data

The obtained experimental results can be compared with resistivity profiles estimated from electromagnetic (EM) and magneto-telluric (MT) field measurements. Recent EM and MT field measurements indicate the existence of high conductivity zones (HCZ) in the crust (Jones, 1992) and in the upper mantle. Partial melting may be one of the plausible explanations of the nature of the HCZ in the lower crust beneath Central Andes, Pyrenees and Tibetan Plateau. With the help of conductivity mixing models it is possible to estimate the amount of melt in the HCZ (see e.g. Glover et al., 2000; Schilling and Partzsch, 2001, and references therein) for MT measurements in Andes, Pyrenees and Tibet. Natural source or magneto-telluric sounding (MT) and controlled source electromagnetism (EM) are two common methods to study the deep electrical structure of the Earth's lithosphere. EM is more appropriate for probing the first hundreds of kilometers below the surface. By using MT, it is possible to probe deeper in the Earth. To probe deeper in the Earth one needs to use EM sounding at lower frequencies. By measuring both magnetic (three components H_x ; H_y ; H_z) and electric (telluric) fields (two component E_x ; E_y) in the Earth and determining their ratio at varying frequencies, it is possible to derive the conductivity variation with both depth and distance. Over a half-space, the apparent resistivity gives the true resis-

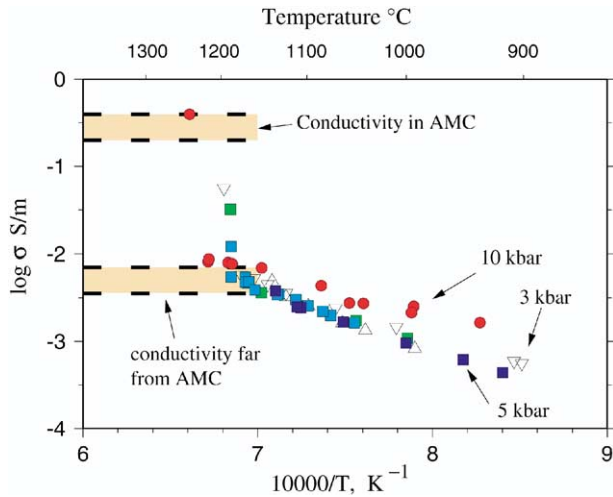


Fig. 13. Oman gabbro conductivity compared to σ , which was estimated in the axial magma chamber in the North Atlantic oceanic ridge by RAMESSES group (Sinha et al., 1998; Heinson et al., 2000).

tivity of the half-space at all frequencies, and a phase lag of 45° . For a multi-layered Earth, these two parameters vary with frequency, and their variation with frequency can be inverted to explain the underlying structure. Partial melting and the effect of the electrical conductivity increase due to the presence of partial melts can be applied to interpret the existing geophysical data on oceanic ridges, like Mid-Atlantic or East-Pacific ridges (see e.g. Forsyth et al., 1998; Sinha et al., 1998; Evans et al., 1999). The measured electrical conductivity of gabbro and peridotites were used to interpret the RAMESSES apparent resistivities (Sinha et al., 1997). This project integrated the both, field MT and EM measurements with the seismic measurements obtained in the northern part of the mid-Atlantic ridge, and demonstrated the existence of two HCZ in the upper mantle and the oceanic crust.

Gabbro samples measured at temperatures below the solidus show the same conductivity range as the conductivity estimated at Reykjanes ridge far from the AMC in the nonmelted lower crust (Fig. 13). The same conclusion can be made for the partially molten gabbro at 1 GPa that exhibits the same conductivity range as that for the conductivity at AMC. Note that the estimated melt fraction measured in this sample after the experiment is ~ 34 vol.%, Table 6, which is similar to the melt fraction estimated in the AMC from RAMESSES project. The conductivity measured in the same sample at 0.5 and 0.3 GPa are 0.5 to 1 order of magnitude lower than estimated AMC conductivity. The Karelia olivinite sample measured at 1 GPa demonstrates melt-free rock conductivity slightly higher than the conductivity of the non-melted crust at Reykjanes ridge (Fig. 14). This is probably due to the high olivine content in the olivinite samples. Partially molten Karelia olivinite shows a conductivity 0.5 order of magnitude higher than the AMC conductivity.

Partially molten lherzolite (Ronda and Spitzbergen peridotites) measured at 1 GPa has a conductivity close to the conductivity range estimated in the partially molten upper mantle rocks below the AMC (Fig. 15) in a source zone. The same observation could be made for the olivine-basalt conductivity

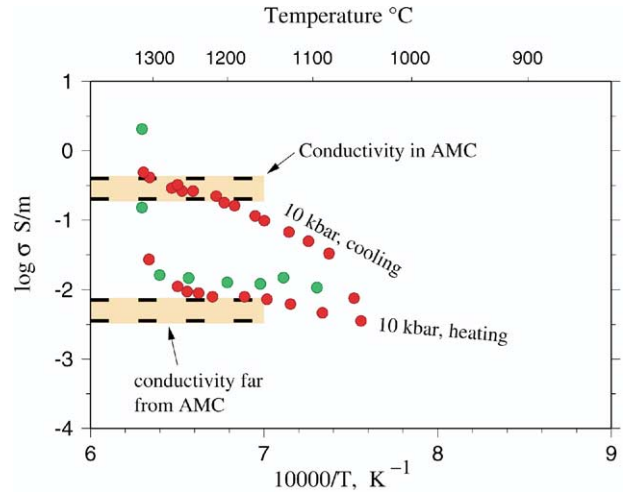


Fig. 14. Karelia olivinite conductivity compared to σ estimated in axial magma chamber in the North Atlantic oceanic ridge by RAMESSES group (Sinha et al., 1998; Heinson et al., 2000).

(Fig. 16). Partially molten Spitzbergen lherzolite measured at 2 GPa is 0.5 order of magnitude more conductive (Fig. 15) than the HCZ below AMC. Here again, there is good agreement between the melt fraction observed in our samples (respectively 11 and 14 vol.% for the Ronda lherzolite and the Spitzbergen lherzolite measured at 1 GPa, Table 6) and the melt fractions estimated in the partially molten mantle in a source zone 60 km below AMC from seismic and electromagnetic data. The discrepancy between these models using experimental data of partially molten rocks with the field measurements of the electrical conductivity from partially molten zones are within the uncertainties of field and laboratory experiments.

5. CONCLUSIONS

This experimental work provides some important insights on the electric conductivity of partially molten mafic and ultra-

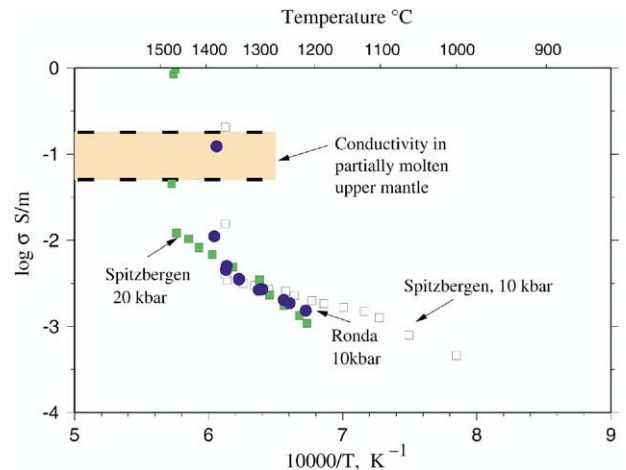


Fig. 15. Spitzbergen and Ronda lherzolite conductivities compared to σ estimated from the partially molten upper mantle below AMC beneath the mid-oceanic Atlantic ridge at 60 km (Sinha et al., 1998; Heinson et al., 2000).

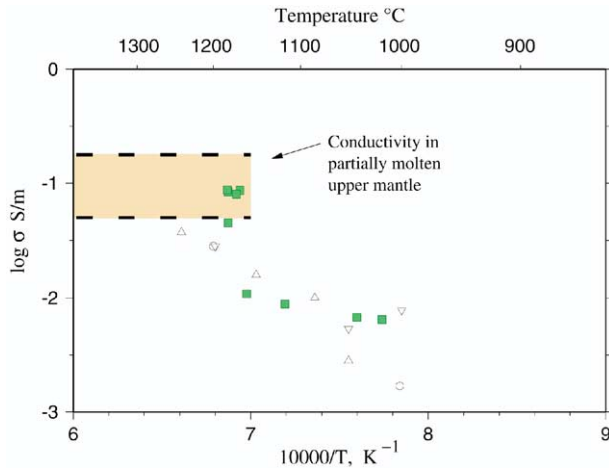


Fig. 16. Olivine + 5 wt.% basalt glass conductivity (squares) compared to Roberts and Tyburczy (1999) (triangles) and σ estimated from partially molten upper mantle below the AMC beneath the mid-oceanic Atlantic ridge at 60 km (Sinha et al., 1998; Heinson et al., 2000).

mafic rocks under pressure up to 2 GPa obtained by complex impedance spectroscopy.

According to our results it can be concluded that:

1. At subsolidus temperatures ($800^{\circ}\text{C} < T < T_{\text{melting}}$), electric conductivity varies according to an Arrhenius expression $\sigma = \sigma_0 \exp(-E_a/kT)$. Pressure does not appear to produce any strong effect on rock electrical conductivity in the experimental pressure range (0.3–2 GPa). $\log \sigma_0$ varies from 0.67 to 2.50 S/m and from 2.65 to 4.25 S/m for crustal and mantle rocks respectively. E_a varies from 0.82 to 1.38 eV and from 2.65 to 4.25 eV for crustal and mantle rocks respectively (see Table 10 for details). Mg number and the relative abundance of olivine and pyroxenes play a decisive role on the electric properties of mafic rocks.
2. When temperature exceeds the solidus temperature, electrical conductivity increases abruptly by 1.5 to 2 orders of magnitude depending on rock conductivity below solidus temperature. This sudden increase of conductivity is not observed at the expected T_s (solidus temperature) but at a slightly higher temperature (at least $\sim 50^{\circ}\text{C}$ above the solidus) and the electric conductivity continues to vary for at least 3 to 4 d due to chemical and textural equilibration of the partial melt before reaching a steady-state value. Melting of samples and the establishment of an interconnected melt network does not influence the semicircular shape of the impedance spectra. The contribution from the grain bound-

Table 10. Electrical conductivity of samples below solidus $\sigma = \sigma_0 \exp(-E_a/kT)$.

Sample	P (GPa)	T ($^{\circ}\text{C}$)	E_a (eV)	σ_0 (S/m)
Oman gabbro	0.3–1	900–1150	1.38	320.54
Karelia olivinite	1	1050–1250	0.82	4.71
Spitzbergen lherzolite	1–2	1250–1400	2.11	$17.68 \cdot 10^3$
Ronda lherzolite	1	1200–1350	1.61	450.34
Olivine San Carlos	1	900–1250	1.53	165.67

ary impedance in samples where grains are in contact with melt can not be recovered from IS measurements.

3. The jump in electrical conductivity at high temperatures was interpreted as the establishment of an interconnected melt network: melts are better electrical conductors than mineral grains. Pressure (that controls solidus temperature) neither influences bulk conductivity, nor its activation energy. The conductivity jump is observed at higher temperatures when the pressure increases according to the pressure dependence of the solidus temperature. SEM study on polished sections of our quenched samples shows that melt/silicates textural equilibrium was reached and that the main conductivity jump is related to the large melt fraction (10–34 vol.%) homogeneously distributed in samples.
4. A direct comparison between these results and those of previous studies of the electric conductivity of partially molten rocks is hindered because of differing measurement strategies. Most of the earlier experiments were performed at 0.1 MPa using either a fixed heating rate (Sato and Ida, 1984; Partzsch et al., 2000) or samples that were texturally equilibrated or sintered at high pressure in separate experiments (Roberts and Tyburczy, 1999). A conductivity jump related to the effect of an interconnected network of melt was also observed in previous studies in which melt fractions were < 5 vol.% (Sato and Ida, 1984; Partzsch et al., 2000). In the present study on rocks containing pyroxenes, no influence of melt on partially molten rock conductivity below a melt fraction of 10 to 15 vol.% was detected. Analysis of our results and Partzsch et al. (2000) by using mixing models of composites (effective media theory, brick layer model, etc.) demonstrate that the electrical conductivity measured in a sample containing < 10 vol.% melt cannot be adequately explained by a completely interconnected melt network nor by a low melt conductivity. For these low melt fractions, bulk conductivity is unaffected due to a lower degree of connectivity (although, the theory of textural equilibrium in partially molten sample predicts that a completely connected network of melt should be reached at a rather low melt fraction even in the case of an anisotropic distribution of interfacial energies at melt/mineral grain interfaces). For melt fractions of 10 to 15 vol.%, melt connectivity is very high and the effect is easily observed by impedance spectroscopy. The variation of electric conductivity in olivine + basalt aggregates does not demonstrate this effect. although we caution that even longer duration of experiments at conditions close to the solidus might indicate otherwise. This point, however, can be considered very important, suggesting that more realistic models to calculate the apparent conductivity of a composite medium consisting of melt and mineral grains are needed in order to better constrain interpretations of MT/EM profiling of partially molten zones in the Earth.

Acknowledgements—Project was supported by German Science Foundation (SPP 1150). The authors are grateful to B. Ildefonse for providing Oman gabbro sample, to F. Brunet for Ronda lherzolite, to A. Loukanin for Kivakka olivinite and Spitzbergen lherzolite, to H. Höfer for technical help with EPMA. The manuscript was significantly im-

proved after the constructive revisions and editing by B. Poe, J. Roberts, and an anonymous reviewer.

Associate editor: B. Poe

REFERENCES

- Admunsen H. E. F., Griffin W. L., and O'Reilly S. Y. (1987) The lower crust and upper mantle beneath nord-western Spitzbergen: Evidence from xenoliths and geophysics. *Tectonophysics* **139**, 169–185.
- Bagdassarov N. (2000) Anelastic and viscoelastic behaviour of partially molten rocks and lavas. In *Physics and Chemistry of Partially Molten Rocks* (eds. N. Bagdassarov, D. Laporte and A. Thompson), pp. 29–65. Kluwer Academic Publishers, Dordrecht, the Netherlands.
- Bagdassarov N. S. and Slutskii A. B. (2003) Phase transformations in calcite from electrical impedance measurements. *Phase Transit.* **76**, 1015–1028.
- Bagdassarov N. S. and Delépine N. (2004) α - β inversion in quartz from low frequency electrical impedance spectroscopy. *Phys. Chem. Solids* **65**, 1517–1526.
- Bagdassarov N., Freiheit H. C., and Putnis A. (2001) Ionic conductivity and pressure dependence of trigonal-to-cubic phase transition in lithium sodium sulphate. *Solid State Ionic* **143**, 285–296.
- Bean V. E. (1983) Fixed points for pressure metrology. In *High Pressure Measurements* (ed. G. N. Pegs), pp. 93–124. Applied Science, London.
- Bohlen S. R. (1984) Equilibrium for precise pressure calibration and a frictionless furnace assembly for the piston-cylinder apparatus. *N. Jab. Miner. MB* **H9**, 404–412.
- Boudier F. (1996) Magma chamber in the Oman Ophiolite: Fed from the top and the bottom. *Earth Planet. Sci. Lett.* **144**, 239–250.
- Brenan J. M. (1993) Diffusion of chlorine in fluid-bearing quartzite: effects of fluid composition and total porosity. *Contrib. Mineral. Petrol.* **115**, 215–224.
- Carmichael R. S. (1982) *Handbook of Physical Properties of Rocks*. CRC Press, Boca Raton, FL.
- Chistiakov A. V., Sharkov E. V., Grokhovskaya T. L., Bogatikov O. A., Muravitskaya G. N., and Grinevich N. G. (2002) Petrology of the Europe largest Burakovka early paleoproterozoic layered pluton (Southern Karelia, Russia) [in Russian]. *J. Earth Sci.* **4**, 1, 35–75.
- Comins M., FitzGerald J. D., Faul U. H., and Green D. H. (1998) A close look at dihedral angles and melt geometry in olivine-basalt aggregates: A TEM study. *Contrib. Mineral. Petrol.* **130**, 336–345.
- Constable S. C. and Duda A. (1990) The electrical conductivity olivine, a dunite, and the mantle. *J. Geophys. Res.* **95**, 6967–6978.
- Constable S. and Roberts J. J. (1997) Simultaneous modeling of thermopower and electrical conduction in olivine. *Phys. Chem. Mineral.* **24**, 319–325.
- Daines M. and Kohlstedt D. L. (1997) Influence of deformation on melt topology in peridotite. *J. Geophys. Res.* **102**, 10257–10271.
- Evans R. L., Tarits P., Chave A. D., White A., Heinson G., Filloux J. H., Toh H., Seama N., Utada H., Booker J. R., and Unsworth M. J. (1999) Asymmetric electrical structure in the mantle beneath the East Pacific Rise at 17°S. *Science* **286**, 752–755.
- Faul U. H. (1997) The permeability of partially molten rocks from experiments and percolation theory. *J. Geophys. Res.* **102**, 10299–10311.
- Forsyth D. W., Webb S. C., Dorman L. M., Orcutt J. A., Harding A. J., Blackman D. K., Morgan J. P., Detrick R. S., Shen Y., Wolfe C. J., Scheirer D. S., Canales J. P., Toomey D. R., Sheehan A. F., Solomon S. C., and Wilcock W. S. D. (1998) Imaging the deep seismic structure beneath a midoceanic ridge: The MELT experiment. *Science* **280**, 1215–1218.
- Fricke H. (1953) The Maxwell-Wagner dispersion in a suspension of ellipsoids. *J. Phys. Chem.* **57**, 934–937.
- Fujii F., Osamura K., and Takahashi E. (1986) Effect of water saturation on the distribution of partial melt in the olivine-pyroxene-plagioclase system. *J. Geophys. Res.* **91**, 9253–9259.
- Ghiorso M. S. and Sack R. O. (1995) Chemical mass transfer in magmatic processes, IV, a revised and internally consistent thermodynamic model for interpretation of liquid solid equilibria in magmatic systems at elevated temperatures and pressures. *Contrib. Mineral. Petrol.* **119**, 197–212.
- Glover P. W. J., Pous J., Queralt P., Muñoz J. A., Liesa M., and Hole M. J. (2000) Integrated two dimensional lithospheric conductivity modelling in the Pyrenees using field scale and laboratory measurements. *Earth Planet. Sci. Lett.* **178**, 59–72.
- Hashin Z. and Shtrikman S. (1962) A variational approach to the theory of effective magnetic permeability of multiphase materials. *J. Appl. Phys.* **33**, 3125–3131.
- Heinson G., Constable C., and White A. (2000) Episodic melt transport at mid oceanic ridges inferred from magnetotelluric sounding. *Geophys. Res. Lett.* **27**, 2317–2320.
- Henstock T. J., Woods A. W., and White R. S. (1993) The accretion of oceanic crust by episodic sill intrusion. *J. Geophys. Res.* **98**, 4143–4161.
- Hirsch L. M. and Shankland T. J. (1993) Quantitative olivine-defect chemical model: Insights on electrical conduction, diffusion, and the role of Fe content. *Geophys. J. Int.* **114**, 21–35.
- Hirsch L. M., Duda A. G., and Shankland T. J. (1993) Electrical conduction and polaron mobility in Fe-bearing olivine. *Geophys. J. Int.* **114**, 36–44.
- Hirschmann M. M. (2000) Mantle solidus: Experimental constraints and the effects of peridotite composition. *Geochem. Geophys. Geosyst.* **1**, 2000GC000070.
- Huebner J. and Dillenburg S. (1995) Impedance spectra of hot, dry silicate minerals and rocks, qualitative interpretation of spectra. *Am. Mineral.* **80**, 46–64.
- Jones A. G. (1992) The lower continental crust. In *Electrical Properties of the Continental Lower Crust* (eds. D. M. Fountain, R. J. Arculus, and R. W. Kay), pp. 81–143. Elsevier, Amsterdam, the Netherlands.
- Khitarov N. I., Slutsky A. B., and Pugin V. A. (1970) Electrical conductivity of basalts at high T-P and phases transitions under upper mantle conditions. *Phys. Earth Planet. Inter.* **3**, 334–342.
- Koptev-Dvornikov E. V., Kireev B. S., Ptschelintzeva N. F., and Khvorov D. M. (2000) Distribution of cumulative paragenesis of major and minor elements in the vertical profile of Kivakka intrusive complex [in Russian]. *Petrologiya* **8**, 6, 631–654.
- Laporte D. and Provost A. (2000) The grain-scale distribution of silicate, carbonate and metallosulphide partial melts: A review of theory and experiments. In *Physics and Chemistry of Partially Molten Rocks* (eds. N. Bagdassarov, D. Laporte and A. Thompson), pp. 93–134. Kluwer Academic Publishers, Dordrecht, the Netherlands.
- Macdonald J. D. (1987) *Impedance Spectroscopy: Emphasizing Solid Materials and Systems*. John Wiley, New York.
- Maxwell J. C. (1881) *A Treatise on Electricity and Magnetism*. Clarendon, Oxford, UK.
- McLachlan D. C., Hwang J. H., and Mason T. O. (2000) Evaluating dielectric impedance spectra using effective media theories. *J. Electroceram.* **5**, 37–51.
- Minarik W. G. and Watson W. G. (1995) Interconnectivity of carbonate melt at low melt fraction. *Earth Planet. Sci. Lett.* **133**, 423–437.
- Nicolas A. (1989) *Structures of Ophiolites and Dynamics of Oceanic Lithosphere*. Kluwer, Dordrecht, the Netherlands.
- Obata M. (1980) The Ronda peridotite: garnet-, spinel-, and plagioclase-lherzolite facies and the P-T trajectory of a high temperature mantle transition. *J. Petrol.* **21**, 533–572.
- Partzsch G. M. (1997) *Elektrische Leitfähigkeit partiell geschmolzener Gesteine: Experimentelle Untersuchungen, Modellrechnungen und Interpretation einer elektrischleitfähigen Zone in den zentralen Anden*. Ph.D. dissertation, Freie Universität Berlin.
- Partzsch G. M., Schilling F. R., and Arndt J. (2000) The influence of partial melting on the electrical behavior of crustal rocks: laboratory examinations, model calculations and geological interpretations. *Tectonophysics* **317**, 189–203.
- Presnall D. C., Simmons C. L., and ?? H. Porath ?? (1972) Changes in electrical conductivity of a synthetic basalt during melting. *J. Geophys. Res.* **77**, 5665–5672.

- Rai C. and Manghnani M. (1977) Electrical conductivity of basalts to 1550°C. In *Magma Genesis Bulletin* (ed. H. Dick), pp. 219–237. Oregon Department of Geol. Miner. Ind, Portland.
- Roberts J. J. and Tyburczy J. A. (1991) Frequency dependent electrical properties of polycrystalline olivine compacts. *J. Geophys. Res.* **96**, 16205–16222.
- Roberts J. J. and Tyburczy J. A. (1993) Impedance spectroscopy of single and polycrystalline olivine compacts: Evidence for grain boundary transport. *Phys. Chem. Miner.* **20**, 19–26.
- Roberts J. J. and Tyburczy J. A. (1999) Partial melt electrical conductivity: Influence of melt composition. *J. Geophys. Res.* **104**, 7055–7065.
- Sakamoto D., Yoshiasa A., Ohtaka O., and Ota K. (2002) Electrical conductivity of olivine under pressure investigated using impedance spectroscopy. *J. Phys. Condens. Matter* **14**, 11375–11379.
- Sato H. and Ida Y. (1984) Low frequency electrical impedance of partially molten gabbro: The effect of melt geometry on electrical properties. *Tectonophysics* **107**, 105–134.
- Scarlato P., Poe B. T., Freda C., and Gatea M. (2004) High pressure and high temperature measurements of electrical conductivity in basaltic rocks from Mount Etna, Sicily, Italy. *J. Geophys. Res.* **109**, B02210.
- Schilling F. and Partzsch G. (2001) Quantifying partial melt fraction in the crust beneath the central Andes and the Tibetan Plateau. *Phys. Chem. Earth* **26**, 239–246.
- Schilling F., Partzsch G. M., Brasse H., and Schwartz G. (1997) Partial melting below the magmatic arc in central Andes deduced from geoelectric field experiments and laboratory data. *Phys. Earth Planet. Int.* **103**, 17–31.
- Schock R., Duba A., and Shankland T. (1989) Electrical conduction in olivine. *J. Geophys. Res.* **94**, 5829–5839.
- Sinha M. C., Navin D. A., MacGregor L. M., Constable S., Peirce C., White A., Heinson G., and Inglis M. A. (1997) Evidence for accumulated melt beneath the slow spreading mid-Atlantic ridge. *Philos. Trans. R. Soc. London, Ser. A* **355**, 233–253.
- Sinha M. C., Constable S. C., Peirce C., White A., Heinson G., MacGregor L. M., and Navin D. A. (1998) Magmatic processes at slow spreading ridges: implications of the RAMESSES experiment at 57°45'N on the mid-Atlantic ridge. *Geophys. J. Int.* **135**, 731–745.
- Toramaru A. and Fujii N. (1986) Connectivity of melt phase in partially molten peridotite. *J. Geophys. Res.* **91**, 9239–9252.
- Tyburczy J. A. and Waff H. S. (1983) Electrical conductivity of molten basalt and andesite to 25 kilobars pressure: Geophysical significance and implications for charge transport and melt structure. *J. Geophys. Res.* **88**, 2413–2430.
- van der Wall D. and Vissers R. L. M. (1996) Structural petrology of the Ronda peridotite, SW-Spain: Deformation history. *J. Petrol.* **37**, 23–43.
- Waff H. S. and Bulau J. R. (1979) Equilibrium fluid distribution in an ultramafic partial melt under hydrostatic stress conditions. *J. Geophys. Res.* **84**, 6109–9114.
- Wagner K. W. (1914) Explanation on the dielectric fatigue phenomenon on the basis of Maxwell's concept. In *Archiv für Electrotechnik* (ed. H. Scherschling). Springer-Verlag, Berlin, Germany.
- Xu Y., Poe B. T., Shankland J. S., and Rubie D. C. (1998) Electrical conductivity of olivine, wadsleyite and ringwoodite under upper mantle conditions. *Science* **280**, 1415–1418.
- Zimmerman M. E. and Kohlstedt D. L. (2004) Rheological properties of partially molten lherzolite. *J. Petrol.* **45**, 275–298.